

Atomic interactions for qubit-error compensations

Michele Delvecchio^{1,2}, Francesco Petiziol^{1,3}, Ennio Arimondo^{4,5}, and Sandro Wimberger^{1,2}

¹Department of Mathematical, Physical and Computer Sciences, University of Parma, Parco Area delle Scienze 7/A, 43124, Parma, Italy

²National Institute for Nuclear Physics (INFN), Milano Bicocca Section, Parma Group, Parco Area delle Scienze 7/A, 43124, Parma, Italy

³Institut für Theoretische Physik, Technische Universität Berlin, Hardenbergstr. 36, 10623 Berlin, Germany

⁴Dipartimento di Fisica E. Fermi, Università di Pisa, Largo. B. Pontecorvo 3, 56127 Pisa, Italy

⁵INO-CNR, Via G. Moruzzi 1, 56124 Pisa, Italy

Experimental imperfections induce phase and population errors in quantum systems. We present a method to compensate unitary phase errors affecting also the population of the qubit states. This is achieved through the interaction of the target qubit with an additional control qubit. We show that our approach can be applied to two and three-level qubit implementations with comparable compensation efficiency.

1 Introduction

Quantum computation is based on a series of unitary transformations applied, *e.g.*, to computational qubits. Quantum states are intrinsically delicate with decoherence being the main limitation. In addition, the unitary transformations associated to quantum gates cannot be implemented with perfect accuracy and their small imperfections will accumulate, leading to a computational failure. Correction schemes must thus protect against those small unitary errors. This error issue is tackled from different directions, for instance, error correction codes [10, 33, 41], composite pulse sequences [25, 29] or quantum control [19–21]. Additional resources are required in all cases: more qubits in the first case, longer times for the qubit preparation and interrogation in the second and additional control fields in the latter. Dynamical phase errors can eventually induce also errors of the qubit-level populations. The ultimate target is to determine and com-

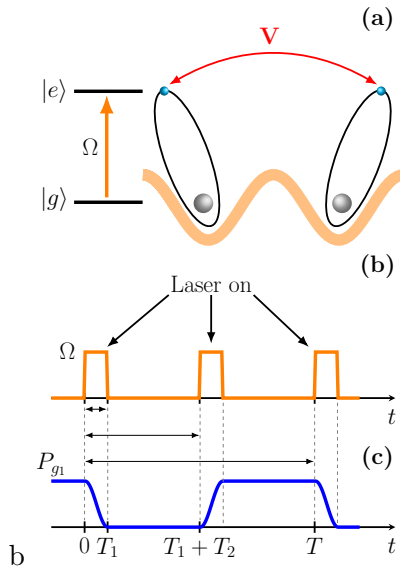


Figure 1: In (a) scheme of two interacting qubits, for instance, two-level Rydberg atoms trapped in an optical potential and experiencing a nearest-neighbour coupling V . They are driven by a common laser field, periodically switched on for the duration T_1 and off for the time T_2 , in a sequence with temporal periodicity $T = 2T_1 + 2T_2$ as schematized in (b). For a perfect excitation, as with π pulses for one-photon absorption, the P_g ground state occupation experiences the temporal evolution shown in (c).

pensate the unwanted phase accumulated in the qubit wavefunction in order to correct coherent (unitary) computational errors.

We introduce here the approach shown in Fig. 1(a), based on the interaction between the "computation" qubit and an additional "correction" qubit, widely used for the implementation of high fidelity quantum-nondemolition measurements [33, 47]. We use the additional phase created by the interaction to compensate for the

Michele Delvecchio: michele.delvecchio@unipr.it

Sandro Wimberger: sandromarcel.wimberger@unipr.it

above unwanted phase in the evolution of the computational qubit. By a proper choice of the interaction strength, we realize compensation for a long sequence of unitary operations of the computational qubit. The compensation efficiency is measured by the wavefunction fidelity reached at the end of the sequence. We obtain a high efficiency for sequence numbers up to fifty. For the long sequence of applied unitary transformations, we derive conditions for the wavefunction phase to maintain the targeted value. In most of the explored qubit level schemes, our approach leads to a magic condition for the required interaction, magic because it creates compensation for a large range of unitary transformation errors.

Our investigation represents a kicked Ising chain of two qubits, longer chains are being investigated for correlations through their level statistics [34]. From the quantum mechanics point of view, our approach is similar to the method of composite pulses. In both cases, the phase of the qubit wavefunction accumulated by the laser-pulse sequence produces a more robust qubit excitation. As main difference, the composite-pulse sequence targets a very large and stable fidelity for a single excitation. We target instead a stable and large fidelity in a long sequence of qubit operations.

The control of the wavefunction phase accumulation has received much attention in different contexts, such as the collapse and subsequent revival of atomic coherence for Bose-Einstein condensates in [31, 32]. Phase correlation destructions and revivals in the time evolution of dipole-blockaded Rydberg states have been investigated under continuous detuned excitation in [14], and for periodic excitation by [15] within the context of discrete time crystals. The quantum control of the phase accumulated by laser driving for interacting Rydberg atoms was studied in [7, 8]. An analysis of laser imperfections in the coherent excitation to atomic Rydberg states was experimentally investigated in [12].

Our qubit interaction is linked to the excited state occupation, for instance in the computation approaches based on atomic Rydberg excitations [1, 27, 37, 49], or on Rydberg-dressed atomic gas [9]. The interaction amplitude depends on the atomic quantum number, and in addition for the Förster resonances the interaction strength tuned by an applied electric field provides a great

control flexibility [7, 22, 23, 35]. Similar interactions occur also in artificial atoms, as the ground state interactions in double quantum dots in a nanowire [40].

The compensation scheme is applied to a computational qubit that, under proper laser handling, experiences a Bloch sphere rotation and reinitialization within a given interrogation temporal interval. We repeat the same operation sequence on a regular basis, and introduce small errors on the laser parameters. Therefore, the qubit accumulates an unwanted phase limiting the computation utility. The compensation recovers its utility through the controlled interaction with the correction qubit. We consider two cases for this qubit, different qubit species or the same one for both qubits. The difference lies in the laser handling error, applied to a single qubit in the first case and to both qubits in the second case. The compensation works out in both cases but the magic value is more stable, producing a larger compensated area with fidelity error of the order of 10^{-6} , for the regimes with two equal qubits.

The compensation is applied to errors in the dynamics of the qubit on a Bloch sphere: rotation angle errors and rotation axis ones, produced by imperfections in the laser intensity and in the laser detuning, respectively. We analyze the one-photon excitation of the two-level qubit by a π laser pulse, allowing a transition at the quantum-speed limit, but with a large sensitivity to the laser excitation parameters [19]. The π pulses are employed for both the qubit excitation and its reinitialization. For a three-level qubit two-photon scheme, we concentrate on the cascade STIRAP configuration [46] with temporal shifted Pump/Stokes laser pulse, providing a large and stable excitation. The application of a double-STIRAP, with inverted Pump/Stokes pulses in the second one, produces the qubit excitation and reinitialization. Similar double-STIRAP pulses are analyzed in [6] for the implementation of quantum logic gates with Rydberg atomic ensembles. In several configurations the three-level STIRAP system may be reduced to a two-level one, where our one-photon compensation scheme may be applied. Instead, we show that the compensation even works in the non-adiabatic regime, where the two level simplification cannot be used [28, 42, 44].

Section II describes the temporal sequence of the computation and reinitialization operations based on the two qubits, the computation and correction one. Such a sequence is repeated for a longer time period allowing the execution of repeated operations. Section III describes the laser driving of the qubits, and introduces the fidelity as a measure of the compensation efficiency. Section IV describes the results of the compensation approach, depending on the form of the excitation, based on either single or two-photon processes. It introduces also an alternative compensation search tool. Results for the laser excitation of only one qubit and both qubits are presented. A final conclusion Section completes our work.

2 Qubit correction

We deal with two $j = 1, 2$ qubits, the first denoted as "computational" qubit and the second one as "correction" qubit. The computational one performs a quantum computation operation and repeats its work n times, with n up to 50 in our simulations. Under laser driving, this qubit starts from the initial ground state $|g_1\rangle$ at time $t = 0$, is excited to the state $|e_1\rangle$ to perform its operation, is reinitialized and is ready for the next round at time $t = T$. A not perfect laser driving leads, at time T , to computation/reinitialization errors that propagate in the operation sequence. We target to compensate for these errors.

Our correction process, schematized in Fig. 1(a), is based on the interaction of the first qubit with the correction qubit. These two qubits, supposed either equal or different, experience in their excited states $|e_j\rangle$ an interaction with controllable amplitude V described by the following Hamiltonian in \hbar units:

$$H_V = V|e_1\rangle\langle e_2\rangle\langle e_1|e_2|. \quad (1)$$

By a proper choice of the interaction amplitude V , the phase introduced into the computational qubit will compensate for laser driving errors.

In our description, the computational process is represented by an elementary step, for instance a rotation of the Bloch vector by a π angle [33]. In this simple approach also the reinitialization is based on a π pulse. The computation/correction sequence is based on the following steps, as in Fig. 1(b). At time $t = 0$, the computational qubit, initially in its ground state, is transferred

to the state $|e_1\rangle$ by a laser pulse of time T_1 . In the following time interval T_2 , the interaction V only determines the qubit evolution. Then an additional laser pulse of duration T_1 transfers the occupation of state $|e_1\rangle$ to the ground state. An interaction of duration T_2 completes the sequence with total time $T = 2T_1 + 2T_2$. Under perfect laser driving, the occupation probability of the ground state of the computational qubit follows the time dependence in Fig. 1(c). More precisely, owing to the parity of the ground/excited states, the laser driving takes place through either a one-photon transition or a two-photon one, with a resonant or non-resonant intermediate level.

We should consider two configurations for the correction qubit. In the main configuration, denoted as two-qubit case, the imperfect laser excitation drives both qubits, producing an equivalence to the Rydberg blockade. Here the Dicke states represent a convenient description basis [2, 11, 17]. Starting from the $|g_1, g_2\rangle$ state at $t = 0$, only the $|e_1, e_2\rangle$ doubly excited state and the $|s\rangle = (|g_1, e_2\rangle + |e_1, g_2\rangle)/\sqrt{2}$ symmetric state are occupied by the laser excitation with no occupation of the antisymmetric Bell/Dicke state. Therefore the wavefunction is written as

$$|\psi_{tot}\rangle = c_{gg}|g_1, g_2\rangle + c_s|s\rangle + c_{ee}|e_1, e_2\rangle. \quad (2)$$

The use of the computational qubit is based on the projection of this wavefunction onto the single qubit space.

In the second case, denoted as one-qubit in the following, the control or correction qubit is different from the computational one. Therefore, the laser excitation does not influence the correction one, *e.g.*, due to a large difference in transition frequency of the two atoms. For instance, for Rydberg atoms in the presence of Förster resonance [35], we may suppose that the correction qubit remains in a long-lived $|e_2\rangle$ state, the interaction being controlled by switching on/off an electric field. The analysis of the one-qubit configuration is a very useful step, because it is simpler since the interaction reduces here just to an effective energy shift of the computation qubit. Nevertheless this case leads to the same general compensation scheme valid also for the two-qubit setup.

3 Qubit laser handles

3.1 Single-photon excitation

For both the one or two-qubit cases, the qubits interact with a laser with detuning $\delta = \omega_L - \omega_0$ from the ω_0 ground/excited state transition and Rabi frequency Ω . The H_{0j} Hamiltonian of each atom ($j = 1, 2$) in the rotating wave approximation in the frame rotating with the drive, is written in units of \hbar as

$$H_{0j} = -\delta|e_j\rangle\langle e_j| + \frac{\Omega}{2} (|g_j\rangle\langle e_j| + |e_j\rangle\langle g_j|). \quad (3)$$

The transfer to the excited states and back is produced by π -pulses with $\delta = 0$, and $\Omega T_1 = \pi$. The ground state occupation reported in Fig. 1(c) is obtained under these conditions.

3.2 Two-photon excitation

In the case of a two-photon excitation, the $|g_j\rangle$ ground and $|e_j\rangle$ ($j = 1, 2$) excited states of a cascade configuration are linked by two laser fields (denoted as Pump and Stokes) through the intermediate state $|i_j\rangle$. The Hamiltonian H_{0j} in a frame doubly rotating at the driving frequencies and in the rotating wave approximation is

$$H_j(t) = \begin{pmatrix} 0 & \frac{\Omega_P(t)}{2} & 0 \\ \frac{\Omega_P(t)}{2} & -\Delta & \frac{\Omega_S(t)}{2} \\ 0 & \frac{\Omega_S(t)}{2} & -\Delta_2 \end{pmatrix}, \quad (4)$$

with Δ the intermediate level detuning, Δ_2 the two-photon detuning, Ω_P and Ω_S the Pump and Stokes Rabi frequencies, respectively. For the resonant STIRAP excitation ($\Delta_2 = 0$) with temporally shifted Pump/Stokes laser pulses [46], the Rabi frequencies have the following Gaussian shaped temporal dependencies:

$$\Omega_P(t) = \Omega_0 e^{-\left(\frac{t-T_1/2}{T_G}\right)^2}, \quad \Omega_S(t) = \Omega_0 e^{-\left(\frac{t+T_1/2}{T_G}\right)^2}, \quad (5)$$

with Ω_0 peak value and width $T_G/\sqrt{2}$. They are parametrized such that the pulse crossing takes place at $t = 0$, and the separation between two subsequent maxima is T_1 . For the transfer back to the ground state with an inverted Pump/Stokes temporal dependencies, the pulse crossing occurs at time $t = T_2$. The time sequence of the laser driving is represented with dashed lines in Fig. 2, please see the right vertical scale for the Rabi frequencies. In order to

maintain generality with respect to the experimental implementations, we work with STIRAP standard dimensionless quantities ΩT_G and ΔT_G . This double-STIRAP sequence has been investigated previously, *e.g.*, in [7, 22].

An efficient and stable STIRAP transfer is realized by imposing an adiabatic evolution of the dark state $|D_j\rangle$ [4, 18] defined as

$$|D_j(t)\rangle = \cos \theta(t) |g_j\rangle - \sin \theta(t) |e_j\rangle, \quad (6)$$

with $\theta(t)$ given by $\tan \theta(t) = \Omega_P(t)/\Omega_S(t)$. If the STIRAP parameters are slowly varied, the qubit initially prepared in the ground state $|g_j\rangle$ follows adiabatically the instantaneous dark state, ending up in the target state $|e_j\rangle$ with very large fidelity. Nonadiabatic coupling between the eigenstates is negligible when the $\theta(t)$ mixing angle rate is smaller than the $\sqrt{\Delta^2 + \Omega_P^2 + \Omega_S^2}$ separation of the Hamiltonian eigenvalues [39]. Robust and efficient STIRAP transfers occur at large values for both Rabi frequencies and intermediate state detuning. There, an adiabatic elimination of the intermediate state leads to an effective two-level system where our one-photon compensation may be applied. Instead, we investigate a nonadiabatic regime where the stability with respect to imperfections in the laser parameter is very limited. This occurs for low Δ values, where the fidelity presents large oscillations as a function of the laser detuning, see, *e.g.*, [45]. This is seen in Fig. 2, where the fidelity $\mathcal{F} = 0.98$ at the end of the first double-STIRAP is not good enough for quantum computation purposes. The complex dependence on Δ will appear below in Fig. 8(a).

3.3 Two-qubit Hamiltonian

Equations (3) and (4) describe single atoms interacting with external fields. We now extend the discussion to two interacting qubits for which the Hamiltonian is the sum of the free-qubit Hamiltonians of those equations and of the inter-qubit interaction of Eq. (1), as reported in Appendix A.

Let us notice important features playing a key role in the compensation process. Both laser detunings and inter-qubit interaction are diagonal terms. From the mathematical point of view, the evolution depends only on the sign conformity of those parameters. This feature will apply also to

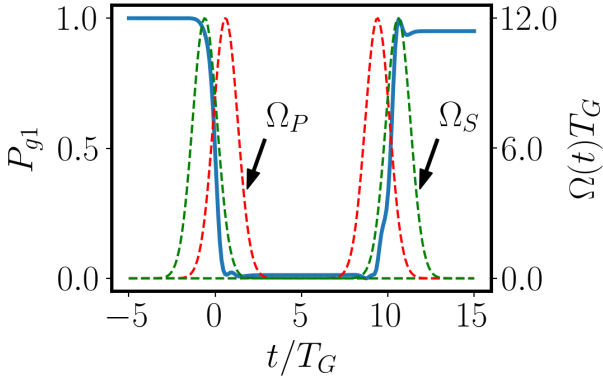


Figure 2: Evolution of the P_{g1} population (blue solid line), and of the Ω_P, Ω_S Rabi frequencies (dashed lines) for a total time T , based on a double-STIRAP transfer sequence to the excited state and back to the ground, as for an atomic Rydberg state. Parameters $T_G = 1$, $T_1 = 1.2$, $\Delta = \Delta_2 = 0$, $\Delta T_G = 1.4$, $\Omega_0 T_G = 12$, and $T_2 = 10$. The P_g occupation scale is on the left, and the $\Omega(t)T_G$ scale is on the right. The P_{g1} temporal evolution over a single T sequence presents the coherent oscillations discussed in [28].

the compensation results. From a physical point of view the diagonal terms may be used to balance each other. This balance occurs in the Rydberg blockade [37], where the interaction is large enough to block the laser excitation to the state $|e_1, e_2\rangle$. Viceversa the tuning of those parameters has been used to enhance that excitation as in the ultracold Rydberg atom antiblockade [3, 5] or in the Rydberg enhancement of a room temperature vapor [26]. We operate with Rabi frequencies of the laser excitation, much larger than the interaction V , where the above processes should *not* occur.

3.4 Fidelity/Infidelity

The efficiency of the correction qubit approach will be measured at the times $t = nT$ by the fidelity \mathcal{F} , or the infidelity $\mathcal{I} = 1 - \mathcal{F}$, between the final and the initial (ground) state $|g_1\rangle$ of the first qubit. For the one-qubit configuration the straightforward fidelity is, given an arbitrary state of the first qubit $|\psi_1\rangle$,

$$\mathcal{F}_1(t = nT) = |\langle g_1 | \psi_1(nT) \rangle|^2. \quad (7)$$

For the two-qubit configuration, the required fidelity is obtained by performing a reduction (partial trace [33]) to the total density matrix. Using the ψ_{tot} wavefunction in the Dicke state basis of

Eq. (2), the fidelity is given by

$$\begin{aligned} \mathcal{F}_2 &= \text{Tr}[(|g_1\rangle \langle g_1| \otimes \mathbb{1}_2)(|\psi_{\text{tot}}\rangle \langle \psi_{\text{tot}}|)] \\ &= |c_{gg}(nT)|^2 + \frac{1}{2}|c_s(nT)|^2. \end{aligned} \quad (8)$$

This fidelity contains the predicted occupation of the computational ground state and an additional term associated to the identity of the two qubits.

4 Fidelity compensation

In typical applications as considered here, the Rabi frequency Ω can be much larger than the interaction V . In this case, the duration T_1 of a π -pulse is much shorter than the time T_2 needed for the interaction to have a sizeable effect. In the limit $T_1 \ll T_2$, it is then justified to treat V as being non-zero only during the interval T_2 . This assumption enables a simpler analytical treatment adopted in the following expressions, while the general configuration is addressed numerically.

4.1 Single-photon

4.1.1 Rotation angle error

For the Rabi π pulse applied over the T_1 time, we introduce a relative error ϵ given by

$$\Omega T_1 = \pi(1 + \epsilon) \quad (9)$$

associated to the Bloch vector rotation angle [33].

At the time $t = T = 2T_1 + 2T_2$, after the first sequence with two π pulses and an acquired phase from the excited state evolution, the ground state fidelity $\mathcal{F}_1(t = T)$ for the one-qubit configuration is

$$\begin{aligned} \mathcal{F}_1(t = T) &= 1 - \frac{1}{2} \sin^2(2\pi\epsilon) [1 + \cos(VT_2)] \\ &\approx 1 - 2(\pi\epsilon)^2 [1 + \cos(VT_2)], \end{aligned} \quad (10)$$

in the second line at small ϵ values. The above expressions report an important feature associated to all the compensation schemes here examined. The $VT_2 = (2m + 1)\pi$ value, with m integer, is "magic" because it produces a strong recovery of the fidelity for the driving error. The excited state phase shift leads to a positive interference in the wavefunction evolution at all the times $t = nT$. At the magic values, the interaction steps preceding and following the second laser pulse produce the exact reverse of the first pulse rotation angle, as shown in Appendix B.

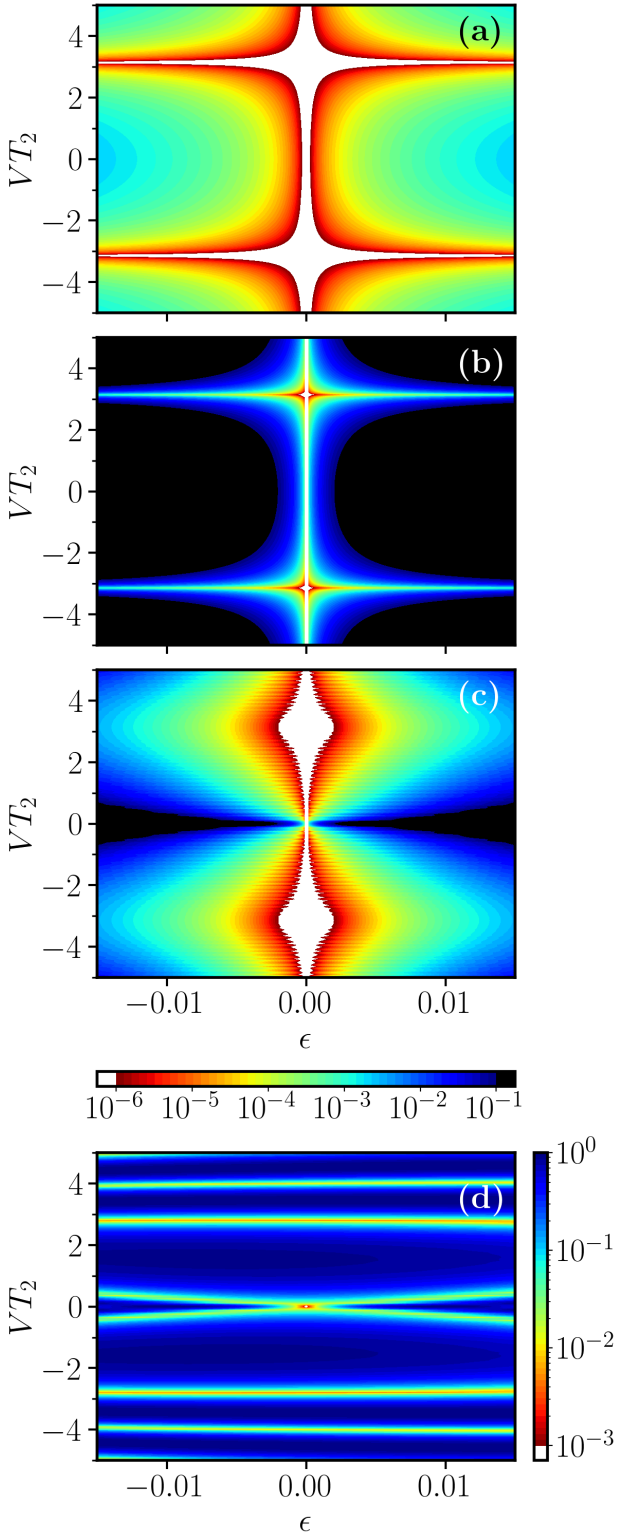


Figure 3: 2D contour plots of the logarithmic scale \mathcal{I} infidelity in the (ϵ, VT_2) plane for a rotation error. The colour scale below (c) applies to the plots (a-c). The black/white regions indicate infidelity values larger/smaller than the color scale limits. Plot of $\mathcal{I}_1(t = T)$ in (a), $\mathcal{I}_1(t = 50T)$ in (b), and $\mathcal{I}_2(t = 50T)$ in (c, d). In (a), and (b) the error compensation corresponds to the one-qubit configuration, in (c, d) to both qubits. In (d) the interaction is continuously active.

The complete qubit sequence reduces to the identity, and the initial state is exactly restored for any value of ϵ . While a full recovery is obtained for all n values at the magic value, Eq. (10) reports a fidelity very close to the one for interaction strengths near the magic value. This phase compensation mechanism has a strong analogy with the spin echo and dynamical decoupling techniques [30, 43], where an arbitrary phase shift is compensated by a double laser excitation. It is also analog to the anti-resonances of the quantum kicked-rotor model where each pulse exactly counteracts the preceding one due to a proper choice of free phase evolution in-between the two pulses [24, 36].

With the laser acting on the computational qubit only, the plots in the (ϵ, VT_2) plane report the resulting infidelity $\mathcal{I}_1(t = T)$ in Fig. 3(a) and $\mathcal{I}_1(t = 50T)$ in (b). These plots, as most of the following ones, are limited on the horizontal to the $|\epsilon| \leq 0.015$ value, easily reached in experiments, and to $|VT_2| \leq 5$ owing to the vertical periodicity (phase) of the compensation. The infidelity range reported in the plots corresponds to standard quantum computation experiments. The plots highlight that the compensation scheme works very well. However, increasing the qubit cycling number, the compensation range around the magic value becomes narrow, and requires a more precise choice of the interaction parameter. The compensation efficiency appears clearly from the data of Fig. 4 where the compensated fidelity \mathcal{F}_1 vs. n is compared to the fidelity reached in multiple operations in the absence of the compensation. For highlighting the robustness of the compensation, notice that the chosen parameter V is only close to the magic value.

The simultaneous driving of both the computation and compensation qubit leads to slightly different features in the time evolution, but the compensation is still produced by the combination of the in-phase laser excitation and the phase acquired here by the state $|e_1, e_2\rangle$ with the laser excitation off. For V off while the laser is on, an analytical solution of the Dicke state time evolution, followed by a projection on the single qubit space, produces the fidelity at time $t = T$ reported in Appendix A with a complex dependence on sine and cosine functions. At small ϵ values the fidelity, from Eqs. (16) and (17), be-

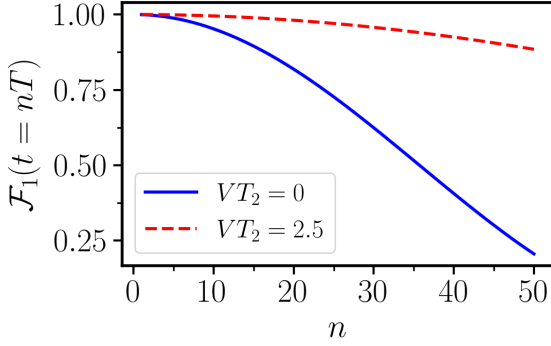


Figure 4: Fidelity $\mathcal{F}_1(t = nT)$ vs. the sequence number n at a given error $\epsilon = 0.007$: in the absence of compensation (solid blue line) and for $VT_2 = 2.5$ (red dashed line) close to the optimal compensation for a laser driving of both qubits.

comes

$$\mathcal{F}_2(t = T) \approx 1 - \frac{1}{2}(\pi\epsilon)^2 [1 + \cos(VT_2)]. \quad (11)$$

Only for one rotation at time $t = T$, the phase shift π remains magic. However, as the number n of interrogations increases, the behavior of the two-qubits configuration is different from the one-qubit case. The two-qubit fidelity remains overall higher than the one-qubit one, as can be appreciated from a comparison between the plots (b) and (c) of Fig. 3. It should be mentioned here that from the time $t = 2T$ onwards the contribution of the Dicke/Bell symmetric state remains below the 10^{-5} level, therefore with an operating compensation, the computational qubit is in perfect shape for continuing its job.

For the case when the interaction V is applied also within the laser excitation period T_1 , the full analytical solution is not available. Therefore we rely on numerical simulations, such as shown in Fig. 3(d), for the two-qubit driving as in all the following figures. The response to the compensation is greatly modified with an optimal compensation that is almost independent of the error ϵ (for the explored range) at new magic values $VT_2 = \pm 2.8$ and $VT_2 = \pm 3.9$. These values converge to the previous magic ones at larger values of the ratio T_2/T_1 .

4.1.2 Compensation search

Although the study of the fidelity at interrogation time nT allows us to identify parameter values giving the desired compensation at $t = nT$,

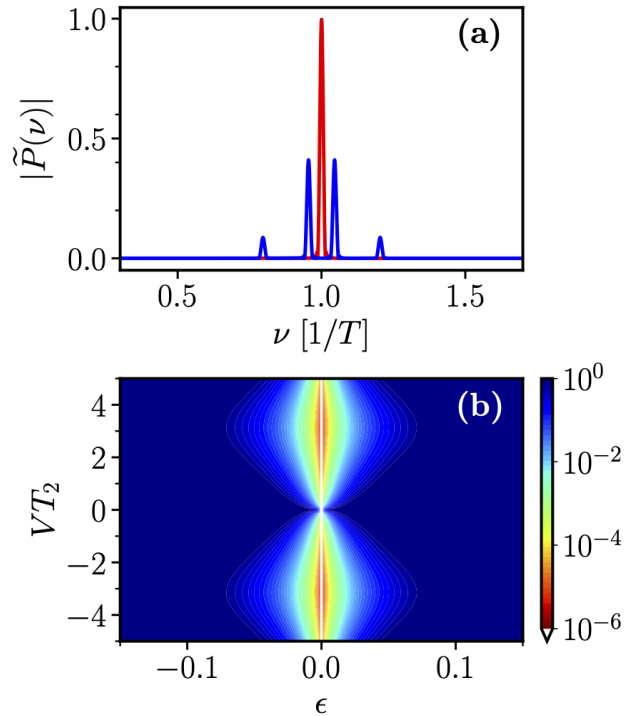


Figure 5: In (a) $|\tilde{P}(\nu)|$ Fourier spectrum of the two-level qubit population difference at $\epsilon = 0.1$ and for $VT_2 = 1$. The sidebands and the splitting are well distinguishable only at these large ϵ values. They coalesce into ν_0 for the magic compensation value, represented schematically by the red curve. In (b) we show $1 - \tilde{P}(\nu_0)$ on a logarithmic scale vs. the parameter plane (ϵ, VT_2) for the rotation error. The white regions indicate infidelity values smaller than the minimum of the color scale.

these values may not guarantee the same fidelity for different n . Therefore, we present now a simple approach for determining the compensation parameters guaranteeing high fidelity during all the interrogations time nT . It is based on the Fourier components of the population difference $P(t) = P_g(t) - P_e(t)$. At $\epsilon = 0$ and at perfect compensation, $P = P_g - P_e$ is a periodic function whose Fourier spectrum contains a single component at $\nu_0 = 1/T$. At the $\epsilon \neq 0$ rotation error, a splitting into two sidebands arises in the population difference Fourier spectrum $\tilde{P}(\nu)$ at the frequencies $\nu_0(1 \pm \epsilon T_1)$, as from the two-level Rabi evolution for π pulses. The interaction V modifies the sideband positions appearing in Fig. 5(a), with a sinusoidal dependence on VT_2 . It also introduces additional weaker sidebands at even larger ϵ values. At the interaction compensation values, the main sideband ideally coalesces into the ν_0 value. The $1 - \tilde{P}(\nu_0)$ amplitude of the Fourier spectrum peak vs. the (ϵ, VT_2) parameters al-

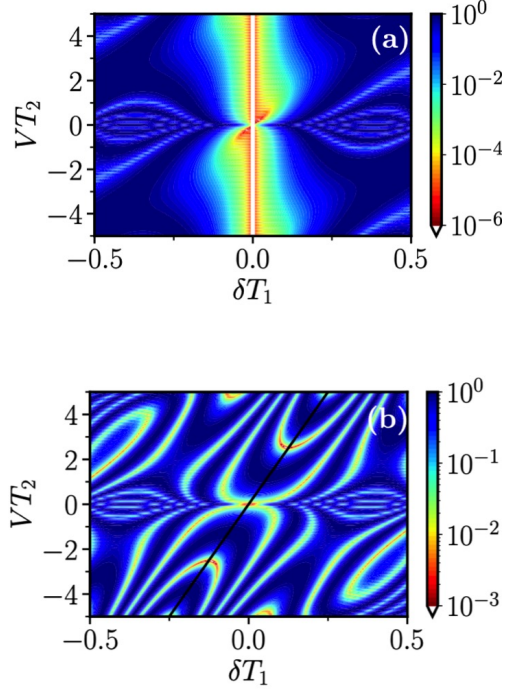


Figure 6: 2D plots of the $\mathcal{I}_2(t = 50T)$ infidelity plot vs. the $(\delta T_1, VT_2)$ parameters for the laser detuning error. Panel (a) is obtained for the case of V off in the periods when the laser is on. In (b) the interaction is on at all times. Here, the tilted black line corresponds to the Rydberg enhancement condition $V = 2\delta$, see main text.

lows a simple determination of the compensation range, as in Fig. 5(b). The analogy between this plot and that of Fig. 3(c) highlights the utility of this search tool in the full parameter space for the compensation.

4.1.3 Rotation axis error

We examine here the compensation of an error associated to the Bloch vector rotation axis [33]. We suppose that the laser detuning error from resonance is given by

$$\delta T_1 = \pi\epsilon. \quad (12)$$

In a π pulse the Bloch vector rotates by the following angle

$$\Omega_{\text{eff}} T_1 = \left[\pi^2 + (\delta T_1)^2 \right]^{1/2} \approx \pi \left(1 + \frac{1}{2}\epsilon^2 \right), \quad (13)$$

to be compared to Eq. (9) of the previous case. For small ϵ values, the fidelity at the time T for the one-qubit configuration is

$$\mathcal{F}_1(t = T) \approx 1 - 2\epsilon^2 [1 - \cos(VT_2)] - \pi\epsilon^3 (2T_2 + 1) \sin(VT_2). \quad (14)$$

Both cosine and sine dependencies on VT_2 appear in the present fidelity. These features lead to the compensation shown in Fig. 6(a). This figure may be compared to Fig. 3(c), also for the horizontal scale owing to the detuning error definition of Eq. (12). Within the central region of low ϵ error, the magic $VT_2 = \pi$ value does not appear clearly. The sine term of Eq. (14) leads to an asymmetric response of the $(\delta T_1, VT_2)$ plot, breaking the analogy with the Rabi error where a δ symmetry is valid for all the ϵ values.

The results for an interaction V acting at all times are shown in Fig. 6(b). The diagonal line dependence of the top figure is greatly enhanced. For a given value of V , the compensation is effective within a more limited range of the detuning error. In order to obtain a wider range of error compensation, the role of V within the laser interaction period is reduced by decreasing the ratio T_1/T_2 .

The diagonal response in Fig. 6(a) for very small values of δT_1 (≈ 0.05) and in (b) globally, is evidence of the Rydberg antiblockade/enhancement. The doubly excited state for the two atoms is reached for $\delta = V/2$, i.e., $\omega_L = \omega_0 + V/2$, taking into account our definition of the interaction energy V provided to the two atoms. This condition corresponds to the black line shown in Fig. 6(b). The excitation of both qubits associated to the enhancement allows for the computational qubit to acquire the phase shift required for the compensation. Notice that, owing to our choice of the laser driving parameters, $\Omega \gg V$, the Rydberg enhancement, and also the blockade, are supposed to be negligible [37]. However, even a weak enhancement may contribute essentially to the more sensitive phase-compensation.

4.2 Double-STIRAP compensation

In the case of the two-photon resonant excitation $\Delta_2 = 0$, we examine the compensation for the non-adiabatic regime in which the fidelity is very sensitive to the intermediate-level detuning Δ . As a consequence of the phase accumulation, such a poorly controlled response is enhanced in a long sequence of double-STIRAP pulses. The rapid decrease of the fidelity with the n number, is shown in Fig. 7(a) where the P_{g1} population of the initial state is plotted vs. time up to $t = 5T$. Driving parameters are as in Fig. 2. An impor-

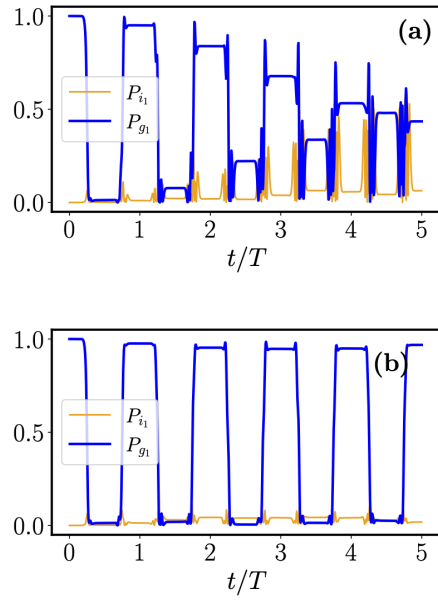


Figure 7: The P_{g1} population (thick blue solid line) and P_{i1} (thin orange line) vs. t time up to $5T$ for a double-STIRAP operation with $\Delta T_1 = 1.4$ and parameters as in Fig. 2. (a) without compensation and (b) with an applied compensation $VT_2 = 2$. Notice the large increase in fidelity produced by the compensation, from $\mathcal{F}_2(t = 5T, V = 0) \simeq 0.43$ to $\mathcal{F}_2(t = 5T, VT_2 = 2) \simeq 0.96$.

tant new feature is the large P_{i1} population occupation of the intermediate state, contributing to less efficient transfer processes with increasing sequence number n . The complex dependence of the infidelity on Δ is presented in Fig. 8(a) evidencing its drastic increase around the value $\Delta T_1 = 1.4$.

We analyze the Fourier spectrum to determine the compensation values when the interaction V is applied at all times. As an example, Fig. 7(b) shows the good and stable fidelity of the computational qubit up $n = 5$ when an interaction compensation $VT_2 = 2$ is applied for the laser parameters of the figure. Very similar results are obtained if the interaction is switched on only for the T_2 periods. The two-dimensional plot in Fig. 8(b) for the central Fourier component vs. the $(\Delta T_1, VT_2)$ parameters, shows the presence of regions where the compensation is very efficient. The compensation remains efficient for a reasonable large range of interaction amplitudes. However, for a maximal compensation, a tuning of the interaction amplitude with the detuning value is required. It should be pointed out that the best compensation is obtained for a sign conformity

between Δ and V , as for the data of Fig. 6. This response suggests a hidden role of the Rydberg enhancement, in appearance not connected to the (δ, V) relation discussed above for the one-photon case. In Fig. 8(b) the tilted parallel lines corresponding to constant compensation reflect the sinusoidal dependence on the parameter VT_2 appearing in the expressions for the fidelity reported above.

5 Conclusions

We have introduced a model for robust quantum control, in which errors affecting a computational qubit are corrected or compensated via the interaction with an additional correction qubit. For the qubit Bloch vector, the standard errors on rotation angle and axis have been considered. Compensation schemes allowing a very efficient recovery of the fidelity are determined. The fidelity remains very high for up to our choice of fifty qubit operations for the parameters investi-

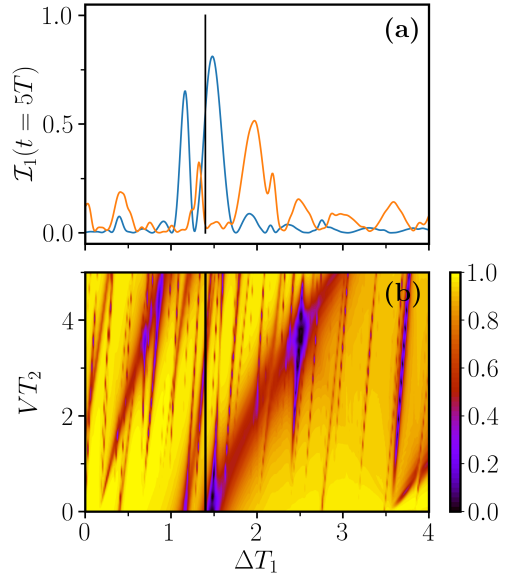


Figure 8: In (a) $n = 5$ infidelities vs. the intermediate level detuning Δ , blue line without compensation and symmetric with respect to the sign of Δ ; orange line for an applied compensation $VT_2 = 2$ and not symmetric with respect to the sign of Δ . The black vertical line marks the $\Delta T_1 = 1.4$ value of Figs. 2 and 7. The other STIRAP parameters are those given in Fig. 2. (b) two-dimensional $(\Delta T_1, VT_2)$ plot of the $1/T$ Fourier spectrum component for the compensation search. The compensation is efficient in different regions of the parameter plane. The black vertical line identifies the $\Delta T_1 = 1.4$ value, as in (a).

tigated here, but longer sequences could be explored on equal footing. An optimal control approach may be used to determine the compensation in the simultaneous presence of both rotation angle and axis errors. For ultracold atomic qubits, the interaction is provided by the Rydberg interactions that represent a very efficient tool for quantum simulations or quantum computation. Using the Förster resonances, the interaction amplitude is easily controlled also with a fast temporal response. In quantum computation, the correction and recovery procedure itself can introduce new errors; the successful fault-tolerant quantum computation [33] can deal with this issue. For most of the explored schemes we have demonstrated that the compensation dependence on the atomic interaction strength is weak. In addition the required corrections are within range typically accessible in experimental realizations, and might help to improve substantially the fidelities reached in novel setups such as based on optomechanics [16].

The quantum control of a long sequence of qubit operations is determined by numerical calculations. However, the examination of the $t = T$ single sequence by analytical calculation, leads to compensation requirements with a precision good enough for exploring longer temporal sequences. Because the compensation efficiency becomes more critical at larger sequence numbers, it should be tuned performing numerical tests.

Our scheme has some analogy with the fidelity increase obtained in quantum gates via Rydberg interactions by driving simultaneously the control and target qubits as examined in [6, 38]. It will be interesting to explore the application of our compensation to quantum gates [8, 48, 49]. The scheme could also be extended to more elaborated STIRAP protocols, as that recently introduced in [13] for artificial atoms. An additional feature to be investigated is the role of qubit dissipation within the times of our compensation.

6 Acknowledgments

One of the authors (E.A.) thanks G. La Rocca and D. Rossini for inspiring discussions. Special thanks goes to G. Falci for a critical reading of the manuscript.

References

- [1] C. S. Adams, J. D. Pritchard, and J. P. Shaffer. Rydberg atom quantum technologies. *J. Phys. B: At. Mol. Opt. Phys.*, 53(1):012002, Dec 2019. DOI: [10.1088/1361-6455/ab52ef](https://doi.org/10.1088/1361-6455/ab52ef). arXiv:1907.09231.
- [2] K. Almutairi, R. Tanaś, and Z. Ficek. Generating two-photon entangled states in a driven two-atom system. *Phys. Rev. A*, 84:013831, Jul 2011. DOI: [10.1103/PhysRevA.84.013831](https://doi.org/10.1103/PhysRevA.84.013831). URL <https://link.aps.org/doi/10.1103/PhysRevA.84.013831>.
- [3] T. Amthor, C. Giese, C. S. Hofmann, and M. Weidmüller. Evidence of antiblockade in an ultracold Rydberg gas. *Phys. Rev. Lett.*, 104:013001, Jan 2010. DOI: [10.1103/PhysRevLett.104.013001](https://doi.org/10.1103/PhysRevLett.104.013001). arXiv:0909.0837.
- [4] E. Arimondo. Coherent population trapping in laser spectroscopy. volume 35 of *Progr. Opt.*, pages 257–354. Elsevier, 1996. DOI: [10.1016/S0079-6638\(08\)70531-6](https://doi.org/10.1016/S0079-6638(08)70531-6). URL <http://www.sciencedirect.com/science/article/pii/S0079663808705316>.
- [5] C. Ates, T. Pohl, T. Pattard, and J. M. Rost. Antiblockade in Rydberg excitation of an ultracold lattice gas. *Phys. Rev. Lett.*, 98:023002, Jan 2007. DOI: [10.1103/PhysRevLett.98.023002](https://doi.org/10.1103/PhysRevLett.98.023002). arXiv:physics/0605111v1.
- [6] I. I. Beterov, M. Saffman, E. A. Yakshina, V. P. Zhukov, D. B. Tretyakov, V. M. Entin, I. I. Ryabtsev, C. W. Mansell, C. McCormick, S. Bergamini, and M. P. Fedoruk. Quantum gates in mesoscopic atomic ensembles based on adiabatic passage and Rydberg blockade. *Phys. Rev. A*, 88:010303, Jul 2013. DOI: [10.1103/PhysRevA.88.010303](https://doi.org/10.1103/PhysRevA.88.010303). arXiv:1212.1138v3.
- [7] I. I. Beterov, D. B. Tretyakov, V. M. Entin, E. A. Yakshina, I. I. Ryabtsev, M. Saffman, and S. Bergamini. Application of adiabatic passage in Rydberg atomic ensembles for quantum information processing. *J. Phys. B: At. Mol. Opt. Phys.*, 53(18):182001, Jul 2020. DOI: [10.1088/1361-6455/ab8719](https://doi.org/10.1088/1361-6455/ab8719). arXiv:2001.06352v1.
- [8] D. D. Bhaktavatsala Rao and K. Mølmer. Robust Rydberg-interaction gates with adiabatic passage. *Phys. Rev. A*, 89:030301, Mar

2014. DOI: 10.1103/PhysRevA.89.030301. arXiv:1311.5147v1.

[9] V. Borish, O. Marković, J. A. Hines, S. V. Rajagopal, and M. Schleier-Smith. Transverse-field Ising dynamics in a Rydberg-dressed atomic gas. *Phys. Rev. Lett.*, 124:063601, Feb 2020. DOI: 10.1103/PhysRevLett.124.063601. arXiv:1910.13687v3.

[10] A. Chiesa, E. Macaluso, F. Petziol, S. Wimberger, P. Santini, and S. Carretta. Molecular nanomagnets as qubits with embedded quantum-error correction. *J. Phys. Chem. Lett.*, 11(20):8610–8615, 2020. DOI: 10.1021/acs.jpclett.0c02213. PMID: 32936660.

[11] D. Comparat and P. Pillet. Dipole blockade in a cold Rydberg atomic sample. *J. Opt. Soc. Am. B*, 27(6):A208–A232, Jun 2010. DOI: 10.1364/JOSAB.27.00A208. arXiv:1006.0742v1.

[12] S. de Léséleuc, D. Barredo, V. Lienhard, A. Browaeys, and T. Lahaye. Analysis of imperfections in the coherent optical excitation of single atoms to Rydberg states. *Phys. Rev. A*, 97:053803, May 2018. DOI: 10.1103/PhysRevA.97.053803. arXiv:1802.10424v1.

[13] P. G. Di Stefano, E. Paladino, T. J. Pope, and G. Falci. Coherent manipulation of noise-protected superconducting artificial atoms in the lambda scheme. *Phys. Rev. A*, 93:051801, May 2016. DOI: 10.1103/PhysRevA.93.051801. arXiv:1509.05562v2.

[14] C.-H. Fan, H.-X. Zhang, and J.-H. Wu. In-phase and antiphase dynamics of rydberg atoms with distinguishable resonances. *Phys. Rev. A*, 99:033813, Mar 2019. DOI: 10.1103/PhysRevA.99.033813. URL <https://link.aps.org/doi/10.1103/PhysRevA.99.033813>.

[15] C.-H. Fan, D. Rossini, H.-X. Zhang, J.-H. Wu, M. Artoni, and G. C. La Rocca. Discrete time crystal in a finite chain of Rydberg atoms without disorder. *Phys. Rev. A*, 101:013417, Jan 2020. DOI: 10.1103/PhysRevA.101.013417. arXiv:1907.03446v2.

[16] V. Fedoseev, F. Luna, I. Hedgepeth, W. Löffler, and D. Bouwmeester. Stimulated Raman Adiabatic Passage in Optomechanics. *Phys. Rev. Lett.*, 126: 113601, Mar 2021. DOI: 10.1103/PhysRevLett.126.113601. arXiv:1911.11464v2.

[17] Z. Ficek and R. Tanaś. Entangled states and collective nonclassical effects in two-atom systems. *Phys. Rep.*, 372 (5):369 – 443, 2002. ISSN 0370-1573. DOI: [https://doi.org/10.1016/S0370-1573\(02\)00368-X](https://doi.org/10.1016/S0370-1573(02)00368-X). arXiv:quant-ph/0302082v1.

[18] M. Fleischhauer, A. Imamoglu, and J. P. Marangos. Electromagnetically induced transparency: Optics in coherent media. *Rev. Mod. Phys.*, 77:633–673, Jul 2005. DOI: 10.1103/RevModPhys.77.633.

[19] L. Giannelli and E. Arimondo. Three-level superadiabatic quantum driving. *Phys. Rev. A*, 89:033419, Mar 2014. DOI: 10.1103/PhysRevA.89.033419. arXiv:1402.1299v1.

[20] S. J. Glaser, U. Boscain, T. Calarco, C. P. Koch, W. Köckenberger, R. Kosloff, I. Kuprov, B. Luy, S. Schirmer, T. Schulte-Herbrüggen, D. Sugny, and F. K. Wilhelm. Training Schrödinger’s cat: quantum optimal control - strategic report on current status, visions and goals for research in europe. *Eur. Phys. J. D*, 69(12): 279, 2015. DOI: 10.1140/epjd/e2015-60464-1. arXiv:1508.00442v1.

[21] D. Guéry-Odelin, A. Ruschhaupt, A. Kiely, E. Torrontegui, S. Martínez-Garaot, and J. G. Muga. Shortcuts to adiabaticity: Concepts, methods, and applications. *Rev. Mod. Phys.*, 91:045001, Oct 2019. DOI: 10.1103/RevModPhys.91.045001. arXiv:1904.08448v2.

[22] G. Higgins, F. Pokorny, C. Zhang, Q. Bodart, and M. Hennrich. Coherent control of a single trapped rydberg ion. *Phys. Rev. Lett.*, 119:220501, Nov 2017. DOI: 10.1103/PhysRevLett.119.220501. URL <https://link.aps.org/doi/10.1103/PhysRevLett.119.220501>. arXiv:1708.06387.

[23] X.-R. Huang, Z.-X. Ding, C.-S. Hu, L.-T. Shen, W. Li, H. Wu, and S.-B. Zheng. Robust Rydberg gate via Landau-Zener control of Förster resonance. *Phys. Rev. A*, 98:052324, Nov 2018. DOI: 10.1103/PhysRevA.98.052324. arXiv:1806.09775v4.

[24] F. M. Izrailev. Simple models of quantum

chaos: Spectrum and eigenfunctions. *Phys. Rep.*, 196(5):299–392, 1990. ISSN 0370-1573. DOI: [https://doi.org/10.1016/0370-1573\(90\)90067-C](https://doi.org/10.1016/0370-1573(90)90067-C).

[25] J. A. Jones. Quantum computing with NMR. *Progr. Nucl. Magn. Res. Spectrosc.*, 59(2):91 – 120, 2011. ISSN 0079-6565. DOI: <https://doi.org/10.1016/j.pnmrs.2010.11.001>. arXiv:1011.1382v1.

[26] D. Kara, A. Bhowmick, and A. K. Moptapatra. Rydberg interaction induced enhanced excitation in thermal atomic vapor. *Scientific Reports*, 8(2):3236, 2018. DOI: <https://doi.org/10.1038/s41598-018-23559-0>. arXiv:1710.05573v1.

[27] H. Labuhn, D. Barredo, S. Ravets, S. de Léséleuc, T. Macrì, T. Lahaye, and A. Browaeys. Tunable two-dimensional arrays of single Rydberg atoms for realizing quantum ising models. *Nature*, 534(769), 2016. DOI: [10.1038/nature18274](https://doi.org/10.1038/nature18274). arXiv:1509.04543v3.

[28] T. A. Laine and S. Stenholm. Adiabatic processes in three-level systems. *Phys. Rev. A*, 53:2501–2512, Apr 1996. DOI: [10.1103/PhysRevA.53.2501](https://doi.org/10.1103/PhysRevA.53.2501). URL <https://link.aps.org/doi/10.1103/PhysRevA.53.2501>.

[29] M. H. Levitt. Composite pulses. *Progr. Nucl. Magn. Res. Spectrosc.*, 18(2): 61 – 122, 1986. ISSN 0079-6565. DOI: [https://doi.org/10.1016/0079-6565\(86\)80005-X](https://doi.org/10.1016/0079-6565(86)80005-X).

[30] D. A. Lidar and T. A. Brun. *Quantum Error Correction*. Cambridge University Press, 2013. DOI: [10.1017/CBO9781139034807](https://doi.org/10.1017/CBO9781139034807).

[31] K. W. Mahmud and E. Tiesinga. Dynamics of spin-1 bosons in an optical lattice: Spin mixing, quantum-phase-revival spectroscopy, and effective three-body interactions. *Phys. Rev. A*, 88:023602, Aug 2013. DOI: [10.1103/PhysRevA.88.023602](https://doi.org/10.1103/PhysRevA.88.023602). arXiv:1304.7565v1.

[32] F. Meinert, M. J. Mark, E. Kirilov, K. Lauber, P. Weinmann, M. Gröbner, and H.-C. Nägerl. Interaction-Induced Quantum Phase Revivals and Evidence for the Transition to the Quantum Chaotic Regime in 1D Atomic Bloch Oscillations. *Phys. Rev. Lett.*, 112:193003, May 2014. DOI: [10.1103/PhysRevLett.112.193003](https://doi.org/10.1103/PhysRevLett.112.193003). arXiv:1309.4045v2.

[33] M. A. Nielsen and I. L. Chuang. *Quantum Computation and Quantum Information*. Cambridge University Press, 2000. ISBN 9780521635035.

[34] C. Pineda and T. Prosen. Universal and nonuniversal level statistics in a chaotic quantum spin chain. *Phys. Rev. E*, 76:061127, Dec 2007. DOI: [10.1103/PhysRevE.76.061127](https://doi.org/10.1103/PhysRevE.76.061127). arXiv:quant-ph/0702164v1.

[35] S. Ravets, H. Labuhn, D. Barredo, L. Béguin, T. Lahaye, and A. Browaeys. Coherent dipole-dipole coupling between two single Rydberg atoms at an electrically-tuned Förster resonance. *Nature Physics*, 10:914, 2014. DOI: [10.1038/nphys3119](https://doi.org/10.1038/nphys3119). arXiv:1405.7804v1.

[36] M. Sadgrove and S. Wimberger. Chapter 7 - A Pseudoclassical Method for the Atom-Optics Kicked Rotor: from Theory to Experiment and Back. volume 60 of *Adv. At. Mol. Opt. Phys.*, pages 315–369. Academic Press, 2011. DOI: <https://doi.org/10.1016/B978-0-12-385508-4.00007-3>.

[37] M. Saffman, T. G. Walker, and K. Mølmer. Quantum information with Rydberg atoms. *Rev. Mod. Phys.*, 82:2313–2363, Aug 2010. DOI: [10.1103/RevModPhys.82.2313](https://doi.org/10.1103/RevModPhys.82.2313). arXiv:0909.4777v3.

[38] M. Saffman, I. I. Beterov, A. Dalal, E. J. Páez, and B. C. Sanders. Symmetric Rydberg controlled- z gates with adiabatic pulses. *Phys. Rev. A*, 101:062309, Jun 2020. DOI: [10.1103/PhysRevA.101.062309](https://doi.org/10.1103/PhysRevA.101.062309). arXiv:1912.02977v3.

[39] B. W. Shore. Picturing stimulated Raman adiabatic passage: a STIRAP tutorial. *Adv. Opt. Phot.*, 9:563–719, 2017. DOI: [10.1364/AOP.9.000563](https://doi.org/10.1364/AOP.9.000563). URL <http://aop.osa.org/abstract.cfm?URI=aop-9-3-563>.

[40] M. Taherkhani, M. Willatzen, E. V. Dening, I. E. Protsenko, and N. Gregersen. High-fidelity optical quantum gates based on type-ii double quantum dots in a nanowire. *Phys. Rev. B*, 99:165305, Apr 2019. DOI: [10.1103/PhysRevB.99.165305](https://doi.org/10.1103/PhysRevB.99.165305).

[41] B. M. Terhal. Quantum error correction for quantum memories. *Rev. Mod. Phys.*, 87: 307–346, Apr 2015. DOI: [10.1103/RevModPhys.87.307](https://doi.org/10.1103/RevModPhys.87.307). arXiv:1302.3428v7.

[42] B. T. Torosov and N. V. Vitanov. Composite stimulated Raman adiabatic passage. *Phys. Rev. A*, 87:043418, Apr 2013. DOI: 10.1103/PhysRevA.87.043418. arXiv:1306.0699v1.

[43] L. Viola, E. Knill, and S. Lloyd. Dynamical decoupling of open quantum systems. *Phys. Rev. Lett.*, 82:2417–2421, Mar 1999. DOI: 10.1103/PhysRevLett.82.2417. arXiv:quant-ph/9809071v2.

[44] N. V. Vitanov and S. Stenholm. Non-adiabatic effects in population transfer in three-level systems. *Opt. Comm.*, 127(4):215 – 222, 1996. ISSN 0030-4018. DOI: https://doi.org/10.1016/0030-4018(96)00216-7.

[45] N. V. Vitanov and S. Stenholm. Properties of stimulated Raman adiabatic passage with intermediate-level detuning. *Opt. Comm.*, 135(4):394 – 405, 1997. ISSN 0030-4018. DOI: https://doi.org/10.1016/S0030-4018(96)00635-9.

[46] N. V. Vitanov, A. A. Rangelov, B. W. Shore, and K. Bergmann. Stimulated Raman adiabatic passage in physics, chemistry, and beyond. *Rev. Mod. Phys.*, 89:015006, Mar 2017. DOI: 10.1103/RevModPhys.89.015006. arXiv:1605.00224v2.

[47] D. F. Walls and G. J. Milburn. *Quantum optics / D.F. Walls, G.J. Milburn*. Springer-Verlag Berlin ; New York, Springer study ed. edition, 1995. ISBN 3540588310.

[48] J.-L. Wu, Y. Wang, J.-X. Han, S.-L. Su, Y. Xia, Y. Jiang, and J. Song. Resilient quantum gates on periodically driven Rydberg atoms. *Phys. Rev. A*, 103:012601, Jan 2021. DOI: 10.1103/PhysRevA.103.012601. arXiv:2101.02328v1.

[49] C. Zhang, F. Pokorny, W. Li, G. Higgins, A. Pöschl, I. Lesanovsky, and M. Hennrich. Submicrosecond entangling gate between trapped ions via Rydberg interaction. *Nature*, 580(7803):345–349, 2020. DOI: 10.1038/s41586-020-2152-9. arXiv:1908.11284v1.

Appendices

A Two-qubit Hamiltonian and fidelity

The aim of this Appendix is to derive the *two-qubit* Hamiltonian, once again for the case where the interaction acts only within the T_2 periods. The solution in the Dicke basis leads to the fidelity of the computational qubit.

Within the single-qubit basis the Hamiltonian is given by the sum of $H_{01} \otimes I + I \otimes H_{02}$, with I the identity matrix and H_{0j} from Eq. (3), and of the interaction term of Eq. (1). As in Sec. 2, the convenient basis to study the present evolution of two qubits is composed by the three symmetric Dicke states of Eq. (2). Within that basis the Hamiltonian is described by the following matrices

$$H_0 = \begin{pmatrix} 0 & \frac{\Omega}{\sqrt{2}} & 0 \\ \frac{\Omega}{\sqrt{2}} & \delta & \frac{\Omega}{\sqrt{2}} \\ 0 & \frac{\Omega}{\sqrt{2}} & 2\delta \end{pmatrix}, \quad H_V = \begin{pmatrix} 0 & 0 & 0 \\ 0 & 0 & 0 \\ 0 & 0 & V \end{pmatrix}, \quad (15)$$

for the laser-on periods and interaction-only periods, respectively. Notice the cooperative $\sqrt{2}$ increase of the Rabi frequency for laser excitation to the symmetric state $|s\rangle$ with respect to Eqs. (3) and (4). For $\delta = 0$, the evolution equations are equivalent to the Bloch equations for a spin-1 system in resonance with the driving field. The interaction produces a VT_2 phase shift of the $|e_1, e_2\rangle$ doubly excited state.

For the calculation of fidelity from Eq. (8) the following Dicke state occupations are required:

$$|c_{gg}(T)|^2 = \frac{1}{4} \left[(1 - \cos(2\Omega T_1)) - \frac{1}{2} (1 - \cos(\Omega T_1))^2 (1 - \cos(VT_2)) \right]^2 + \frac{1}{16} [1 - \cos(\Omega T_1)]^4 \sin^2(VT_2) \quad (16)$$

$$|c_s(T)|^2 = \frac{1}{4} \sin^2(\Omega T_1) \left[\cos^2(\Omega T_1) (5 + 3 \cos(VT_2)) + (2 \cos(\Omega T_1) + 1) (1 - \cos(VT_2)) \right]. \quad (17)$$

Using Eq. (8) the fidelity at time ($t = T$) is obtained as

$$\mathcal{F}_2(t = T) = |c_{gg}(T)|^2 + \frac{1}{2}|c_s(T)|^2. \quad (18)$$

Iterating such a procedure, one can obtain analytical expressions of the fidelity at periods $n > 1$. However, due to its growing complexity, a software such as Mathematica is helpful for obtaining the rather lengthy algebraic expressions with increasing n .

B One-qubit configuration with $VT_2 = \pi$

The present target is to derive the magic compensation value from the temporal evolution of the two-level single qubit, with time separated actions of laser and interaction. For the case of rotation angle error with an arbitrary Rabi frequency Ω including the ϵ error as from Eq. (9), the evolution operator at time $T = 2T_1 + 2T_2$ is

$$U(T) = e^{-iVT_2|e_1\rangle\langle e_1|} e^{-i\frac{\Omega T_1}{2}\sigma_{x1}} e^{-iVT_2|e_1\rangle\langle e_1|} e^{-i\frac{\Omega T_1}{2}\sigma_{x1}} \quad (19)$$

with σ_{x1} the Pauli matrix for the computational qubit. We demonstrate that for $VT_2 = \pi$ the operator $U(T)$ corresponds to the identity matrix, for all the Ω values.

Let us consider the first three exponentials in Eq. (19) r.h.s.. Written in matrix form, they explicitly read

$$\begin{pmatrix} e^{-iVT_2} & 0 \\ 0 & 1 \end{pmatrix} \begin{pmatrix} \cos(\frac{\pi}{2}(1+\epsilon)) & -i\sin(\frac{\pi}{2}(1+\epsilon)) \\ -i\sin(\frac{\pi}{2}(1+\epsilon)) & \cos(\frac{\pi}{2}(1+\epsilon)) \end{pmatrix} \begin{pmatrix} e^{-iVT_2} & 0 \\ 0 & 1 \end{pmatrix}, \quad (20)$$

Setting $VT_2 = \pi$ and performing the matrix product, we obtain

$$\begin{pmatrix} \cos(\frac{\pi}{2}(1+\epsilon)) & i\sin(\frac{\pi}{2}(1+\epsilon)) \\ i\sin(\frac{\pi}{2}(1+\epsilon)) & \cos(\frac{\pi}{2}(1+\epsilon)) \end{pmatrix} = e^{i\frac{\Omega T_1}{2}\sigma_x}. \quad (21)$$

This operator performs a rotation of the Bloch vectors equal and opposite to that induced by the first pulse of the sequence in Eq. (19). Inserting the latter result in that equation we obtain

$$U(T) = e^{i\frac{\Omega T_1}{2}\sigma_x} e^{-i\frac{\Omega T_1}{2}\sigma_x} = I, \quad (22)$$

demonstrating the magic value compensation, independent of the ϵ rotation angle error.

The application of the evolution operator to the case of the rotation axis error unfortunately does not produce a similar simple interpretation since both errors cannot be exactly corrected by the same procedure from above. One may apply, however, an optimal control approach to find the optimal value for the best simultaneous compensation of both errors.